Experimental study of the effect of roughness and Reynolds number on fluid flow in rough-walled single fractures: a check of local cubic law

Jiazhong Qian,[1] Zhou Chen,[1] Hongbin Zhan[2,3]* and Houchun Guan[4]

[1] *School of Resources and Environmental Engineering, Hefei University of Technology, Hefei 230009, China*
[2] *Department of Geology and Geophysics, Texas A & M University, College Station, TX 77843-3115, USA*
[3] *Faculty of Engineering and School of Environmental Studies, China University of Geosciences, Wuhan 430074, China*
[4] *Anhui Institute of Geological Survey, Hefei 230009, China*

Abstract:

Local cubic law (LCL) is one of the most commonly applied physical laws for flow in single fractures (SF) and fractured media. The foundation of LCL is Darcian flow. This experimental study examines if LCL is valid for flow in a single rough fracture and how the fracture roughness and Reynolds number (Re) affect flow. Similar to the Moody diagram for flow in pipes, a diagram for flow in a single rough fracture has been generated to relate the friction coefficient with Re and the roughness. Under the experimental condition of this study, flow appears to be substantially different from Darcian flow. The flow law of $q \propto e^n J^m$ appears to be valid for describing the flow scheme where q, e, and J are the unit width flux, the average aperture, and the hydraulic gradient. The value of the power index m is found to be around $0.83 \sim 0.98$, less than what has been used in Darcian flow ($m = 1$). The power index n is around 11.2 and 13.0, much greater than the n value used in the LCL ($n = 3$), and it increases with the average velocity. The Moody type of diagram shows that the friction factor for flow in SFs is influenced by Re and the roughness. It decreases with Re when Re is small, and becomes less sensitive to Re when Re is large enough. It also increases with the roughness. Copyright © 2010 John Wiley & Sons, Ltd.

KEY WORDS   variable rough-walled fractures; groundwater flow; Moody diagram; experimental study; non-Darcian flow

Received 4 December 2009; Accepted 22 July 2010

INTRODUCTION

Flow and transport in a single fracture (SF) have been a focus of research in hydrology, petroleum engineering, and other disciplines for many decades because of their importance in various applications including nuclear waste repository (Lomize, 1951; Louis, 1969; Witherspoon *et al.*, 1980; Pyrak-Nolte *et al.*, 1987; Zimmerman *et al.*, 1991; Zimmerman and Bodvarsson, 1996; Konzuk and Kueper, 2004; Ranjith and Darlington, 2007; Nowamooz *et al.*, 2009). Despite enormous progress made, some basic aspects of flow in an SF still remain unstudied (Berkowitz, 2002). From a rigorous theoretical point of view, flow in an SF should be investigated with the Navier–Stokes equation (NSE) (Zimmerman and Bodvarsson, 1996). Unfortunately, the full NSE is often too difficult to solve, either analytically or numerically (Zimmerman and Yeo, 2000). As a result, only a handful of studies have been reported on the numerical simulation of the NSE in an SF (Brush and Thomson, 2003; Al-Yaarubi *et al.*, 2005; Cardenas *et al.*, 2007) and even fewer studies on the analytical solutions of the NSE in an SF (Hasegawa and Izuchi, 1983; Basha and El-Asmar, 2003). Therefore, various approximations

are usually made, which reduce the NSE to a simplified equation. A commonly employed simplification is to discard the acceleration term in the NSE, which yields the linear Stokes equation (SE) (Zimmerman and Bodvarsson, 1996; Zimmerman and Yeo, 2000). The condition for this simplification is that the Reynolds number (Re) is less than a certain limit, which is often chosen to be 10 (Zimmerman and Yeo, 2000). Although the SE is linear, it is still quite difficult to solve and only a few studies have been devoted to solve the SE in an SF (Brown *et al.*, 1995; Mourzenko *et al.*, 1995; Brush and Thomson, 2003). The next simplification is to replace the SE by the lubrication equation or the so-called 'local cubic law' (LCL) (Brown, 1987; Zimmerman and Yeo, 2000). The LCL states that the fluid volumetric flow rate in a fracture is proportional to the fracture aperture to the power of three. The condition for this simplification is that the wavelength of the dominant aperture variations is more than three times greater than the mean aperture (Zimmerman and Yeo, 2000). Other investigators such as Oron and Berkowitz (1998) gave somewhat similar conditions for simplifying the NSE to the SE and to the lubrication equation or LCL.

Because of its simplicity, the LCL has been studied extensively and has become the primary governing law for flow in an SF (Iwai, 1976; Brown, 1987; Moreno *et al.*, 1988; Thompson and Brown, 1991; David, 1993;

* Correspondence to: Hongbin Zhan, Department of Geology and Geophysics, Texas A & M University, College Station, TX 77843-3115, USA. E-mail: zhan@geo.tamu.edu

Unger and Mase, 1993; Amadei and Illangasekare, 1994; Brush and Thomson, 2003; Nazridoust *et al*., 2006). In a rigorous sense, the LCL works the best for Darcian flow in a highly idealized SF with smooth and parallel fracture surfaces (Lomize, 1951; Louis, 1969). Unfortunately, field observations indicate that natural fractures are very unlikely to have smooth and parallel surfaces (Meheust and Schmittbuhl, 2001). Witherspoon *et al*. (1980) tested the validity of the LCL in an SF where the surfaces were in contact and the aperture was being decreased under stress using samples of granite, basalt, and marble. They concluded that the LCL was valid whether the fracture surfaces were held open or being closed under stress; the effects of deviations from the ideal parallel plate concept could be dealt with by using a reduced geometric factor (Witherspoon *et al*., 1980). This conclusion was based on Darcian flow in an SF. Konzuk and Kueper (2004) pointed out that the cubic law calculated with either the geometric mean aperture or incorporating surface roughness factors provided reasonable (±10%) estimates of the observed flow rates for *Re* less than 1. The LCL over-predicted the observed flow rates by at least 1·9 times. Konzuk and Kueper (2004) further pointed out the merit in conducting additional studies of the cubic law applied at the single-fracture scale to determine whether similar results were achievable in all fracture types.

The LCL will become invalid when either of the two conditions that lead the NSE to the SE and to the lubrication equation is not satisfied. When *Re* increases to more than 10 and/or the wavelength of the dominant aperture variations is less than three times the mean aperture, one may see the deviation from the LCL. This theoretical argument was supported by mounting computational (Skjetne *et al*., 1999; Basha and El-Asmar, 2003; Bues *et al*., 2004; Koyama *et al*., 2008) and experimental evidences (Lomize, 1951; Louis, 1969; Raven and Gale, 1985; Pyrak-Nolte *et al*., 1987; Durham and Bonner, 1994; Keller *et al*., 1995; Vandergraaf, 1995; Qian *et al*., 2005, 2006, 2007) which showed that the LCL was not adequate when flow velocity was high and/or fracture roughness increased. Durham and Bonner (1994) used profilometry to show that flow channels became more torturous as joint faces approached one another and permeability of an SF dropped faster than the parallel plate approximation predicted. Cook (1992) also showed that flow through a fracture decreased more rapidly than the cube of the mean aperture. Ranjith and Darlington (2007) found a Forchheimer-type quadratic relationship between the flow rate and the pressure change when modelling water flow through a real rock fracture at confining pressures from 0·55 to 3·0 MPa. Similarly, Zimmerman *et al*. (2004) reported that at *Re* above about 20, both the simulations and experiments exhibited a Forchheimer-type regime, in which the pressure drop was quadratic in the flow rate.

Lomize (1951) showed that for Darcian flow in an SF, the flow rate was proportional to the cube of the aperture; however for turbulent flow, the flow rate was proportional to 1·5 power of the aperture. Louis (1969) further studied groundwater flow in an SF with the condition $\Delta/e > 0·033$, where Δ is the asperity height of the fracture surface and e is the fracture aperture. His finding was similar to that of Lomize (1951). Pyrak-Nolte *et al*. (1987) reported a comprehensive experimental study of the mechanical and hydraulic behaviour of natural fractures in crystalline rock under normal stress and concluded that the LCL did not hold at either high or low stresses for natural fractures, as has also been found by Raven and Gale (1985). Pyrak-Nolte *et al*. (1987) concluded that the flow rate was proportional to the mechanical aperture in a single, nature fracture to a power index varying between 7·6 and 9·8. Sisavath *et al*. (2003) found that a power-law relationship can be obtained between the flow rate and the average aperture with an exponent as high as 10, which is consistent with the finding of Pyrak-Nolte *et al*. (1987). Xu *et al*. (2003) studied water flow in a rough SF made of steel and concluded that the power index of flow rate was between 5·5 and 7·6 for a non-inosculated fracture. As can be seen from the above references, a wide range of power index values has been reported for various fracture flow problems.

To test if the LCL is valid or not, a very important issue is to choose the 'average' fracture aperture in the formula. Unfortunately, the geometric complexity of a real fracture may cause some ambiguity on this issue and there are still considerable debates on what 'average' aperture to use for simulating flow and transport in an SF (Tsang, 1992; Ge, 1997; Oron and Berkowitz, 1998). Tsang (1992) illustrated that some discrepancy among different results of flow and transport in an SF was due to different choices of the average aperture and she provided a careful analysis of different definitions of fracture aperture. Ge (1997) used two vectorial variables of fracture geometry (true aperture and tortuosity) to study flow in an SF. Oron and Berkowitz (1998) argued that the cubic law aperture should not be measured on a point-to-point basis but rather as an average over a certain length.

The purpose of this study is to experimentally investigate flow in an SF when *Re* is considerably greater than 10. In order to avoid any unnecessary ambiguity in interpreting the experimental data and to precisely control the parameters in the experiments, we use a parallel-plane SF with glued identical square plates on one surface to simulate the fracture roughness. We are aware that this artificially made SF is an idealized one, i.e. different from a realistic SF with variable apertures. But its aperture and surface roughness can be precisely controlled; thus, the ambiguity of choosing the average fracture and surface roughness is avoided. In fact, a similarly idealized SF has been used in other studies as well. For instance, Fourar and Lenormand (2001) generated an artificial SF by gluing a layer of glass beads to two glass plates to study two-phase flow at high velocities through such an SF. Bues *et al*. (2004, Figure 1) studied flow in an SF with rectangular corrugation or roughness. One goal of this study is to examine a generic relationship between the flow rate and the hydraulic gradient for flow in an
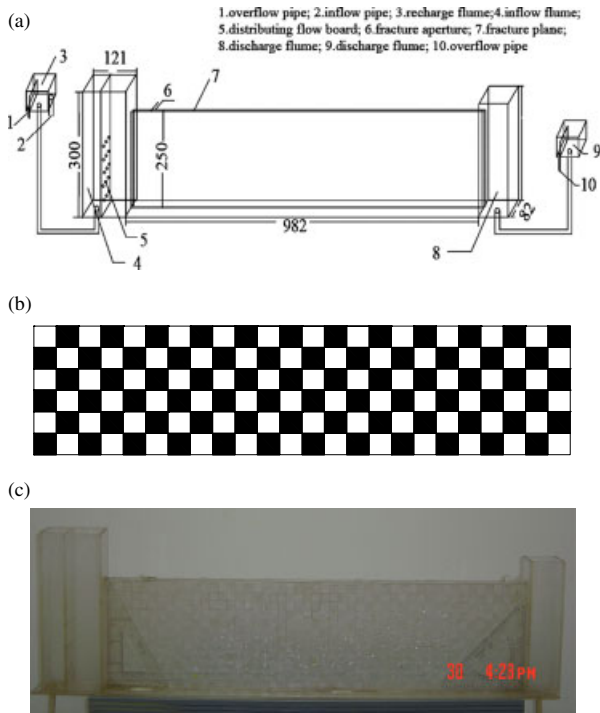
Figure 1. Diagram showing the friction factor as a function of *Re* and the roughness for flow in SFs. This diagram is similar to the Moody diagram used to describe flow in pipes
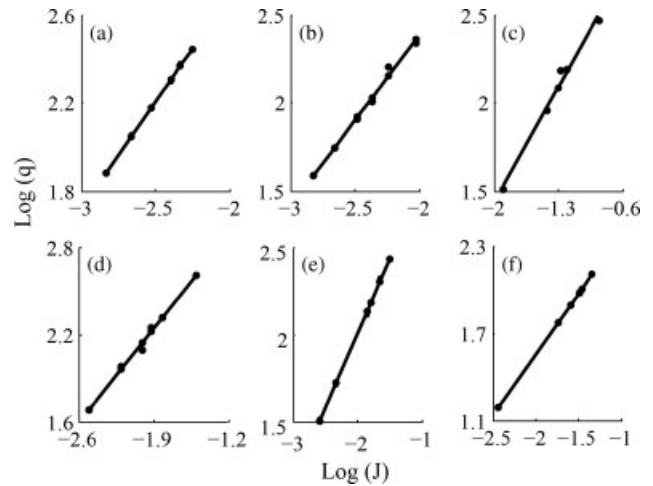

Figure 2. (a) Schematic diagram of experimental set-up for groundwater flow in an SF. 1, overflow pipe; 2, inflow pipe; 3, high-level recharge flume providing different constant water level; 4, inflow flume; 5, distributing flow board; 6, fracture aperture; 7, fracture plane; 8, discharge flume; 9, low-level discharge flume providing different constant water level; and 10, overflow pipe; (b) schematic diagram of roughness design on one of the fracture surfaces. The rough surface is constructed through gluing different square plexiglass plates to the black squares; and (c) photograph of the apparatus set-up

SF based on various controlled surface roughnesses. A diagram similar to the Moody diagram for flow in pipes will be generated for flow in an SF (Munson *et al*., 1998). The finding of this study can be used as a benchmark to compare with further studies using a realistic SF.

EXPERIMENTAL DESIGN

A series of experiments have been performed on an artificial SF constructed in the laboratory. Figure 2a shows the general design of the experiments. The fracture is constructed between two plexiglass plates of dimensions 982 mm in length and 250 mm in width. The hydraulic gradient through the fracture is controlled by adjusting the water level difference between the inflow and the outflow flumes. The range of the hydraulic gradient is between 0·015 and 0·046, as shown in Table I. The fracture is vertical and open at the top; thus an unconfined flow condition exists. The vertical fracture used here is different from the horizontal fractures used in other studies such as the one by Iwai (1976). However, the conclusions are not expected to depend on the orientation of the fracture except that confined flow exists for a horizontal fracture, whereas unconfined flow exists for a vertical fracture. Because the hydraulic gradient used in the experiment is small enough over the distance of flow, the nonlinear effect of the unconfined flow is negligible.

Figure 2b is a schematic diagram showing the design of the rough fracture surface. The rough surface is constructed by gluing many identical small plexiglass plates to the center of the black areas with dimensions of 40 mm × 40 mm. Six different plexiglass plates have

been used to represent six different roughnesses, namely pattern 1 to pattern 6. These six patterns have dimensions of 40 mm × 40 mm × 1 mm (pattern 1), 40 mm × 40 mm × 2 mm (pattern 2), 40 mm × 40 mm × 3 mm (pattern 3), 20 mm × 20 mm × 1 mm (pattern 4), 20 mm × 20 mm × 2 mm (pattern 5), and 20 mm × 20 mm × 3 mm (pattern 6). The detail of design is as follows. First, keep one of the two fracture surfaces smooth, and the other one to be glued with different plates selected from patterns 1 to 6. When gluing the plates to the black squares of Figure 2b, make sure the sides of the plates are parallel to those of the black squares and the plate is at the center of the black square occupied. For patterns 1−3, the glued square plates will cover the entire black squares of Figure 2b, whereas for patterns 4−6, the glued square is smaller and only covers the central part of each black square. A photograph of the actual set up is shown in Figure 2c.

After making the rough fracture surface, mounting the rough and smooth surfaces vertically in the apparatus and making sure they are parallel, an artificial rough SF is constructed. The asperity height of the fracture, Δ, is the thickness of the glued plates. For instance, for patterns 1, 2, and 3, the values of the asperity heights are 1, 2, and 3 mm, respectively. Similarly, the values of the asperity heights for patterns 4, 5, and 6 are also 1, 2, and 3 mm, respectively. The roughness is given by Δ/e, where e is the average aperture defined as

$$e = \frac{\text{Vol}_f}{\frac{1}{2}(h_1 + h_2)l} \tag{1}$$

where Vol_f is the water volume contained in the fracture (m^3), h_1 and h_2 are the water levels at the recharge and discharge flumes, respectively (m), and l is the distance

Table I. Values of the discharge per unit width (*q*) *versus* the hydraulic gradient (*J*) with different fracture patterns

Fracture	e (mm)	Δ/e	Experiment No.	J	q (mm²/s)
Pattern 1	4·90	0·204	1	0·0015	75·19
			2	0·0022	114·44
			3	0·0030	151·76
			4	0·0041	198·89
			5	0·0047	239·19
			6	0·0056	273·55
Pattern 2	4·50	0·444	1	0·0015	38·60
			2	0·0022	56·00
			3	0·0033	81·12
			4	0·0043	101·66
			5	0·0058	161·26
			6	0·0094	219·06
Pattern 3	3·78	0·794	1	0·0126	32·46
			2	0·0379	90·87
			3	0·0500	122·03
			4	0·0533	152·59
			5	0·0621	156·63
			6	0·1407	293·16
Pattern 4	4·80	0·208	1	0·0031	47·65
			2	0·0063	95·61
			3	0·0099	124·72
			4	0·0120	175·09
			5	0·0152	208·84
			6	0·0313	404·51
Pattern 5	4·24	0·472	1	0·0026	33·05
			2	0·0047	51·40
			3	0·0141	129·41
			4	0·0162	149·13
			5	0·0225	209·74
			6	0·0319	275·38
Pattern 6	3·84	0·781	1	0·0037	15·64
			2	0·0183	59·68
			3	0·0256	77·12
			4	0·0324	93·48
			5	0·0350	100·82
			6	0·0460	128·83

between the entrance and exit of the fracture. h_1 and h_2 are very close to the top elevation of the fracture. Vol_f and the average flow velocity (*V*) are monitored using a calibrated cylinder with errors less than 2%, and h_1 and h_2 are measured using pressure transducers with errors less than 0·5 mm. Under steady-state flow condition, the hydraulic gradient, *J*, is given by

$$J = \frac{h_1 - h_2}{l} \qquad (2)$$

Rigorously speaking, the hydraulic gradient of an unconfined flow system changes with distance from the two constant-head boundaries; however, the difference between h_1 and h_2 are very small, as can be seen from Table I. Thus Equation (2) is a reasonably good approximation of the hydraulic gradient. The unit width flux (m²/s), denoted as *q*, is also measured as $q = Q/[(h_1 + h_2)/2]$, where *Q* is the total discharge rate through the fracture and $(h_1 + h_2)/2$ is the averaged saturated width of the fracture. The difference between h_1 and h_2 is very small, so $(h_1 + h_2)/2$ is very close to h_1

(or h_2). Note that the unit width flux *q* is different from the specific discharge which equals to *q/e*.

PROPOSED FLOW LAW

Theoretical background of the proposed flow law

The LCL is based on the following Darcian flow

$$q = \frac{ge^3}{12\nu}J \qquad (3)$$

where *q* is the unit width flux (m²/s), *e* is the average aperture (m), *g* is the acceleration of gravity (m/s²), ν is the kinematic viscosity (m²/s), and *J* is the hydraulic gradient. Lomize (1951) modified Equation (3) for Darcian and turbulent flow by considering fracture roughness. The one for Darcian flow is

$$q = \frac{ge^3}{12\nu}J\frac{1}{1 + 6(\Delta/e)^{1.5}} \qquad (4)$$

where Δ/e is the roughness.

Pyrak-Nolt *et al.* (1987) modified Equation (3) as

$$q = q_0 + Ce_m^n \qquad (5)$$

where q_0 is a background constant unit width flux (m²/s), e_m is the mechanical aperture, *n* is a power index which varies from 7·6 to 9·8, and *C* is a unit converting the constant coefficient with a dimension of m$^{(2-n)}$/s. Xu *et al.* (2003) summed up the models mentioned above and obtained the following formula:

$$q = C'\frac{ge^n}{12\nu}J^m\frac{1}{1 + \xi(\Delta/e)^\eta} \qquad (6)$$

where *n*, *m*, and η are the dimensionless power indexes of *e*, *J*, and Δ/e, respectively; ξ is a dimensionless coefficient of (Δ/e), C' (m$^{(3-n)}$) is a unit converting constant to make sure the unit to the right-hand side of Equation (6) is consistent with that of *q*. The use of C' here is similar to the use of '*C*' in Equation (5) by Pyrak-Nolt *et al.* (1987). Equation (6) is a generic formula that incorporates many previous equations as special cases. Since porosity of the SF is unity, *q* is related to the average flow velocity *V* as

$$V = q/e \qquad (7)$$

In the following, we will adopt Equation (6) to explain the experimental data.

Numerical analysis

In order to use Equation (6), one needs to develop a procedure for identifying three power indexes *n*, *m*, and η, and one coefficient ξ based on the experimental data. The parameter C' is simply a constant to make sure the units on both sides of Equation (6) are consistent; thus it is not discussed in the following. We will determine *m* first, *n* second, and η and ξ together last. If non-Darcian flow occurs, which is likely for high-speed flow in an

SF, the relationship between q and J is nonlinear and m is not 1. To find the value of m from experimental data, taking logarithm on both sides of Equation (6) leads to

$$\log\ q = m\ \log\ J + \log\ G \qquad (8)$$

where

$$G = \frac{C'ge^n}{12\nu[1 + \xi(\Delta/e)^\eta]} \qquad (9)$$

G is a characteristic parameter related to the aperture and surface roughness of the fracture. In some sense, G can be regarded as a 'non-Darcian' conductivity coefficient of the fracture. Similar but slightly different terminology has been used by Wen *et al.* (2006) to describe the power-law non-Darcian flow. One way to find the value of m is to plot q *versus* J in a log–log paper. If a straight line can be identified from the plot, the slope of that straight line will yield the value of m. Substituting Equation (9) into Equation (8) leads to

$$\log\ q = n\ \log\ e - \log[1 + \xi(\Delta/e)^\eta] + (m\ \log\ J$$
$$+ \log(C'g) - \log(12\nu)) \qquad (10)$$

To determine n, one needs to conduct the experiments with different values of e, which is obtained via Equation (1) and to plot q *versus* e in a log–log paper. If a straight line can be identified from such a plot, then the slope of that straight line is the value of n.

To determine η and ξ, one needs a different approach. Here we have employed an optimization procedure based on Equation (10). This procedure is briefly explained as follows. Reorganizing Equation (10) as

$$\log[1 + \xi(\Delta/e)^\eta] = n\ \log\ e$$
$$+ \left(m\ \log\ J + \log(C'g) - \log(12\nu)\right) - \log\ q\ (11)$$

where all the terms on the right-hand side of Equation (11) are known except the constant C'. The idea is to start with some initial guessing values of η, ξ, and C' and then to minimize the difference between the left-hand side of (11) with the right-hand side of (11) until reaching the global minimum after several iterations. The optimization procedure is accomplished with a Matlab program and the optimized values are obtained.

EXPERIMENTAL RESULTS AND DISCUSSION

Relationship between q and J

On the basis of experimental results, the unit width flux (q) is measured. The average aperture (e) and the hydraulic gradient (J) are obtained through Equations (1) and (2), respectively. The results are summarized in Table I. We then try to interpret the data using Equation (6), following the procedures described in the Section on Numerical Analysis. The exponent m of each pattern fracture is first determined and the result is listed in Table II. The associated statistical properties such as the correlation coefficient (γ) and the standard deviation

(SD) are also summarized in Table II. The relationships between q and J for patterns 1–6 are drawn in log–log plots in Figure 3a–f. To see if the obtained m value is related to the roughness Δ/e, Figure 4 is plotted, where Case (a) is for patterns 1–3 and Case (b) is for patterns 4–6. One should be aware that the purpose of Figure 4 is to identify the trend, not to precisely determine the functionality of m and Δ/e. To serve this purpose, a minimum of three data points are acceptable for identifying the trend.

Table II shows that the values of m lie in 0·98 and 0·83 for patterns 1–6. The largest m value is for pattern 1 which has the smallest roughness, whereas the smallest m value is for pattern 6 which has the largest roughness. For patterns 1 and 2, the m values are close to 1, indicating that flow is close to Darcian. For patterns 3–6, the m

Table II. The values of the exponent m of each pattern fracture and their statistical analysis

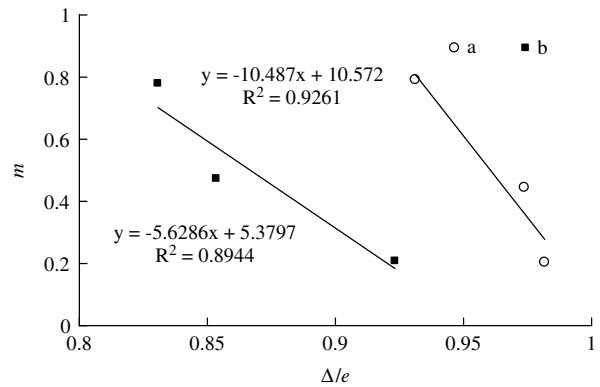| Fracture	m	Correlative coefficient (γ)	Standard deviation (SD)
Pattern 1	0·98	0·999	0·0087
Pattern 2	0·97	0·995	0·0289
Pattern 3	0·93	0·992	0·0431
Pattern 4	0·92	0·997	0·0280
Pattern 5	0·85	0·999	0·0170
Pattern 6	0·83	0·999	0·0057

Figure 3. Log–log plots of the unit width flux (q) *versus* the hydraulic gradient (J) in different fractures
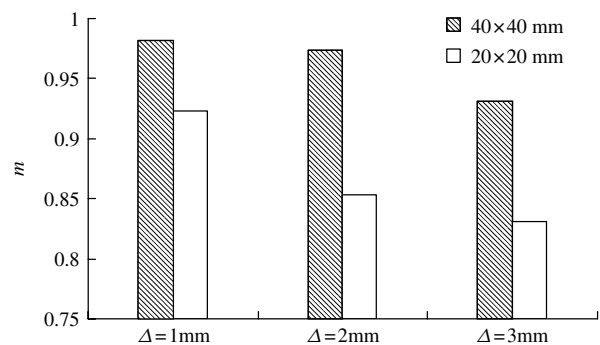

Figure 4. Plots of the power index m in Equation (6) *versus* the roughness (Δ/e). Case (a) there is for patterns 1–3 (40 mm × 40 mm) (open circles) and Case (b) is for patterns 4–6 (20 mm × 20 mm) (black squares)

values become increasingly smaller than 1, indicating a trend of deviation from Darcian flow. Table II also shows the nearly perfect correlation between q and J^m, reflected in the correlation coefficients that are very close to 100%. The excellent correlation between q and J^m is also seen from Figure. 3a–f. The slope of the simulated line represents the m value.

Table II and Figure 4 also show that the values of m vary with the roughness (Δ/e) in different fractures. The value of m decreases from 0·98, 0·97, to 0·93 when the pattern changes from 1 to 3 [Figure 4, Case (a)]. Similarly, the value of m decreases from pattern 4 to 6 as well [Figure 4, Case (b)]. This observation is expected. As the roughness increases, flow within the fracture deviates further from the Darcian flow, and becomes more turbulent, manifested by a decreasing m value from unity (Darcian).

Another interesting phenomenon observed is that the m value is smaller for pattern 4 than that for pattern 1 (Figure 5); both even have the same asperity height (1 mm). Similar conclusions can be drawn when comparing results for patterns 5 and 2, or patterns 6 and 3 (Figure 5). The shaded bars in Figure 5 are for patterns with 40 mm by 40 mm, whereas the white bars in Figure 5 are for patterns with 20 mm × 20 mm. However, we do not expect that such findings can be extended to extremely large or small percentages of roughness coverage of the fracture surface. For instance, when the roughness coverage is approaching 100%, meaning that the entire fracture surface is covered with plates, then that fracture plane actually becomes 'smooth' and homogeneous again. On the contrary, when the roughness coverage is approaching 0% also, the fracture plane is nearly smooth and homogeneous. Flow in either of these two extremes is expected to be more close to Darcian than flow in patterns 1–6, provided that the rest conditions remain the same in the experiments.

Relationship between q, e, and Δ/e

Using the procedures described in the Section on Numerical Analysis, the value of n is determined by plotting q *versus* e in a log–log paper and the results are shown in Tables III and IV, where Table III is for

Table III. Values of n, ξ, and η for rough squares of dimension 40 mm × 40 mm in the fracture

J	N	ξ	η
0.0015	11·24	40·34	22·57
0.0022	11·52	32·18	19·06
0.0030	11·70	8·11	19·66
0.0041	11·73	−0·30	0·27
0.0056	11·92	−0·32	0·27

Table IV. Values of n, ξ, and η for rough squares of dimension 20 × mm × 20 mm in the fracture

J	n	ξ	η
0.0015	11·86	23·86	0·53
0.0022	12·20	33·17	0·62
0.0030	12·48	43·45	0·68
0.0041	12·75	55·28	0·76
0.0056	13·00	69·32	0·83

patterns 1–3 and Table IV is for patterns 4–6. After this, the values of η and ξ are obtained using the optimization procedure of the Section on Numerical Analysis and the results are also shown in Tables III and IV. The unit converting constant C' in Equation (6) is less relevant to our discussion, and thus is not included in the discussion. Figure 6a shows the relationship between n and J for patterns 1–3, and Figure 6b shows the relationship between n and J for patterns 4–6. Several observations can be made. Firstly, the n values in Tables III and IV are approximately between 11·2 and 13·0, which are much greater than 3 (the cubic law); meaning that flow is substantially deviated from LCL in such fractures. Secondly, the value of n increases with the value of J; meaning that a greater hydraulic gradient will lead to greater deviation from the LCL.

The n value found in this study is greater than what has been reported in previous studies. For instance, Pyrak-Nolte *et al.* (1987) reported n values ranging from 7·6 to 9·8. Nevertheless, the experimental set-up, in particular, the design of the fracture roughness varies from study to study, but our finding of the n values in the range 11·2–13·0 implies that flow in a single rough fracture
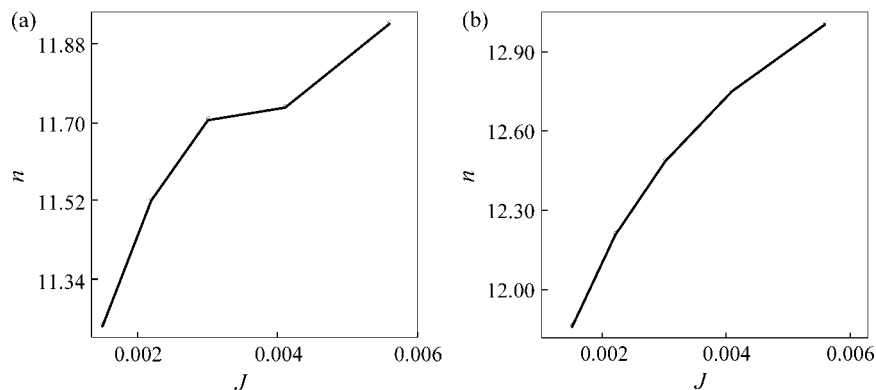

Figure 5. Plots of the power index m in Equation (6) *versus* different asperity height (Δ) for patterns 1–3 (40 mm × 40 mm) in shaded bars and patterns 4–6 (20 mm × 20 mm) in white bars
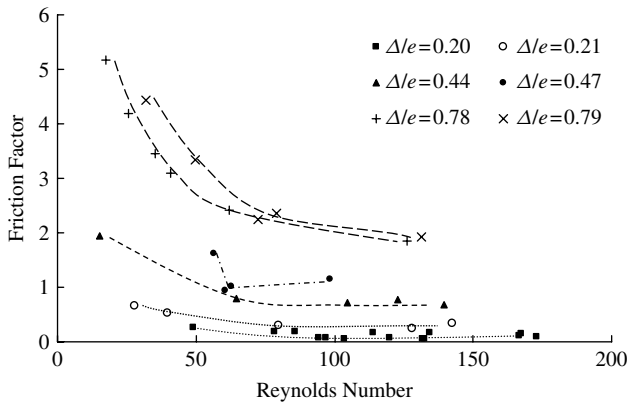
Figure 6. Plots of the power index n in Equation (6) *versus* the hydraulic conductivity (J) for (a) patterns 1–3 (40 mm × 40 mm) and (b) patterns 4–6 (20 mm × 20 mm)

could be much different from what one can expect from the Darcian flow. The large n value also implies that flow is sensitive to the aperture e which is defined specifically in Equation (1). We must point out that because different investigators may use different ways to define and measure the aperture, it is possible that different flow laws will result from the same set of experimental data. In terms of the second observation that the value of n increases with the value of J; one can argue that a greater J value indicates stronger turbulent flow or greater deviation from Darcian flow, thus a larger n value.

One notable point from Tables III and IV is that the values of ξ and η vary over broader ranges than those of m and n. This is particularly true for results shown in Table III. This implies that the form of $1/(1 + \xi(\Delta/e)^{\eta})$ in Equation (6) is probably not a good choice for describing fracture roughness in Table III. Notice that the difference between Tables III and IV is the size of plates used to simulate fracture roughness. Table III has a larger size of plates, thus flow in those fractures of Table III is expected to be more tortuous than those in Table IV. This indicates that when the degree of flow tortuosity increases in an SF, the credibility of Equation (6) decreases.

DISCUSSION

Discussion of Re

The value of Re is calculated via (Qian *et al.*, 2005)

$$Re = \frac{Ve}{2\nu} \qquad (12)$$

where V is the average flow velocity in the fracture. The values of Re are calculated for patterns 1–6. For instance, the values of Re are found to be 33·86 and 36·58 for flow in fractures with pattern 1 and pattern 6 roughnesses (Table I). The range of Re is consistent with those of Iwai (1976), Schrauf and Evans (1986), and Zimmerman and Yeo (2000) who showed that turbulent flow can occur in an SF for Re greater than 10. However, the flow scheme does not depend on Re alone. The surface roughness

is another important factor to consider. Therefore, the flow scheme will at least depend on both Re and the surface roughness for flow in SFs. In fact, in the literature for studying flow in pipes, it has long been recognized that the flow scheme is a function of both Re and the surface roughness. The broadly used Moody diagram in fluid mechanics graphically shows such a relationship (Munson *et al.*, 1998).

Diagram of friction coefficient of flow on Re and the roughness

It is desirable to generate a diagram for flow in SFs similar to the Moody diagram for flow in pipes. With such a diagram as a reference, one can tell different flow schemes qualitatively and calculate flow discharge quantitatively, based on Re and the surface roughness. One may argue that the existing Moody diagram for flow in pipes as shown in Munson *et al.* (1998) may be useful for interpreting flow in SFs as well. However, without experimental evidence to support, one is not sure if the Moody diagram for flow in pipes is valid, or at least, sufficiently accurate for dealing with flow in SFs, because pipes and SFs have very different geometries. Unfortunately, such a diagram for flow in SFs does not exist in the literature to our knowledge.

In the following, we attempt to generate such a diagram for flow in SFs, similar to what was done for flow in pipes (Munson *et al.*, 1998). Ideally, one likes to generate such a diagram with a wide range of flow velocity and Re. Unfortunately, the range of the flow velocity and Re reported in this study are not broad enough to cover the entire evolution of flow from laminar, to partially turbulent, then to fully developed turbulent flow. Additional experimental studies are needed in the future to augment the diagram of this study for such a purpose. The procedure of generating such a diagram is as follows.

Substituting Equation (6) into Equation (7) leads to

$$V = C' \frac{ge^{n-1}}{12\nu} J^m \frac{1}{1 + \xi(\Delta/e)^{\eta}} \qquad (13)$$

Because $J = \Delta h/l$, where Δh is the hydraulic head loss ($\Delta h = h_1 - h_2$) and l is the distance of flow, Equation (13) is written as follows:

$$\Delta h = \left\{ \frac{12\nu[1 + \xi(\Delta/e)^{\eta}]}{C'ge^{n-1}} \right\}^{\frac{1}{m}} lV^{\frac{1}{m}} \qquad (14)$$

When flow is Darcian, m is 1; when flow is fully turbulent, m is 0·5; and when flow is partially developed turbulent (transitional turbulent), m has a value between 0·5 and 1. Whatever the case, Equation (14) can be expressed as the Darcy–Weisbach type of equation

$$\Delta h = f_w \frac{lV^2}{2gR} \qquad (15)$$

where R is the hydraulic aperture and f_w is the friction coefficient which is a function of Re and the roughness $f_w = f_w(R_e, \Delta/e)$ (Louis, 1969). For flow in an SF,

Qian *et al.* (2005, Equation (3)) have shown that $R = e/2$ when recognizing the fact that the aperture e is much smaller than h_1 or h_2. Therefore, Equation (15) is modified to

$$f_w = \frac{ge\Delta h}{lV^2} \qquad (16)$$

We use Equation (16) to calculate f_m for each of the six patterns 1–6, and to plot f_m as a function of Re and the roughness. The result is shown in Figure 1. Several features can be identified from this figure. First, f_m is obviously influenced by Re and the roughness. Second, for the same Re, f_m increases with the roughness. Third, for the same roughness, f_m decreases with Re at first, but when Re is large enough, f_m is less sensitive to the change of Re. Two bands of curves are observed in Figure 1. One has the friction factor below 2 and the other above 2. The friction factor curve for roughness of 0·47 is abnormal and is less reliable. The exact reason for this unusual behaviour is not clear but could be caused by measurement errors. The diagram generated in Figure 1 is in some degree similar to the Moody diagram generated for flow in circular pipes (Munson *et al.*, 1998).

If needed, a diagram showing the fracture hydraulic conductivity, K, as a function of Re for different fracture roughness can be generated based on Figure 1 and Equation (15). Reformulating Equation (15) into the form of Darcy's law, one has $K = \frac{2gR}{f_w V}$.

The discussion of friction factor here is focused on the power-law type of the flow law. This is a reasonable choice because the range of Re in the experiments is quite small [about one order of magnitude, Figure (1)]. If the range of Re is over a few orders of magnitude, it is probably better to use the Forchheimer type of flow law. This is a subject that deserves further study in the future.

About the surface roughness

There are a few interesting issues related to surface roughness that can be explored in the future. Firstly, although different patterns of roughness are used in this study, the rough and smooth elements were regularly installed. This may generate another research topic, i.e. with the same roughness, will the conclusion change when the roughness plates are randomly rather than orderly distributed? Our hypothesis is that the conclusion here is not sensitive to the spatial arrangement of the rough element, but it is sensitive to the pattern of the roughness used. Furthermore, if different roughness patterns coexist in an SF, which pattern will influence the flow law the most? This question is a little difficult to answer, but we hypothesize that the roughness element with greater thickness will have greater influence on the flow law. Secondly, the roughness patterns used in this experiment are squares with sharp corners which can easily generate turbulent flow and cause great resistance to flow as well. If the roughness patterns have shapes without sharp corners such as elliptical or circular plates, it will be harder to generate turbulent flow and flow resistance will be smaller as well. We hypothesize that the

flow law will be closer to the LCL for such roughness, provided that the rest conditions remain unchanged. Testing the hypotheses discussed above will lead to the choice of an adequate flow law for flow in a natural SF under high Re.

SUMMARY AND CONCLUSIONS

The focus of this experimental study is to examine how the surface roughness and Re affect flow in an SF and if the LCL is valid for flow there. The roughness of the fracture is made by gluing identical plates following a regular order on one of the fracture surfaces. Two different square sizes of 40 mm × 40 mm and 20 mm × 20 mm with three different thicknesses of 1, 2, and 3 mm have been used to generate six different roughness patterns. The artificially made SF is then mounted vertically in a tank and connected with two constant-head flumes to establish steady-state horizontal flow in the fracture. Various flow discharges have been created to examine the flow schemes under various Re values and fracture roughness. Similar to the Moody diagram for flow in pipes, a diagram for flow in an SF has been generated to relate the friction coefficient with Re and the roughness. The following conclusions can be summarized from this study. This study can be a benchmark for further study of flow in a natural SF under high Re.

1. Under the experimental condition of this study, flow appears to be substantially different from the Darcian flow. The flow law of $q = C' \frac{ge^n}{12\nu} J^m \frac{1}{1 + \xi(\Delta/e)^\eta}$ appears to be valid for describing the flow scheme. The value of the power index m is found to be around $0·83 \sim 0·98$, less than what has been used in Darcian flow ($m = 1$). The m value deviates more from unity when the roughness becomes greater. The credibility of this flow law decreases when the flow tortuosity in the SF increases.
2. The power index n of the above flow law is around 11·2 and 13·0, which is much greater than the n value used in the LCL. The value of n is found to increase with the average velocity for a given roughness of fracture.
3. The Moody type of diagram shows that the friction factor for flow in SFs is influenced by Re and the roughness in the following fashion. It decreases with Re when Re is small and becomes less sensitive to Re when Re is large enough. It also increases with the roughness.

REFERENCES

Al-Yaarubi AH, Pain CC, Grattoni CA, Zimmerman RW. 2005. Navier–Stokes simulations of fluid flow through a rock fracture. In *Dynamics of Fluids and Transport in Fractured Rocks*, Fabishenko B, Witherspoon PA, Gale J (eds). American Geophysical Union: Washington, DC; 55–64.

Amadei B, Illangasekare T. 1994. A mathematical model for flow and solute transport in non-homogeneous rock fractures. *International Journal of Rock Mechanics and Mining Sciences and Geomechanics Abstracts* 31(6): 719–731.

Basha HA, El-Asmar W. 2003. The fracture flow equation and its perturbation solution. *Water Resources Research* 39(12): 1365. DOI: 10.1029/2003WR002472.

Berkowitz B. 2002. Characterizing flow and transport in fractured geological media: a review. *Advances in Water Resources* 25: 861–884.

Brown SR. 1987. Fluid flow through rock joints: the effect of surface roughness. *Journal of Geophysical Research* 92(B2): 1337–1347.

Brown SR, Stockman HW, Reeves SJ. 1995. Applicability of the Reynolds equation for modeling fluid flow between rough surfaces. *Geophysical Research Letter* 22(18): 2537–2540.

Brush DJ, Thomson NR. 2003. Fluid flow in synthetic rough-walled fractures: Navier–Stokes, Stokes, and local cubic law simulations. *Water Resources Research* 39(4): 1085. DOI: 10.1029/2002WR001346.

Bues M, Panfilov M, Crosnier S, Oltean C. 2004. Macroscale model and viscous-inertia effects for Navier–Stokes flow in a radial fracture with corrugated walls. *Journal of Fluid Mechanics* 504: 41–60.

Cardenas MB, Slottke DT, Ketcham RA, Sharp JM. 2007. Navier–Stokes flow and transport simulations using real fractures shows heavy tailing due to eddies. *Geophysical Research Letter* 34: L14404. DOI: 10.1029/2007GL030545.

Cook NGW. 1992. Natural joints in rock: mechanical, hydraulic and seismic behaviour and properties under normal stress. *International Journal of Rock Mechanics and Mining Sciences and Geomechanics Abstracts* 29: 198–223.

David C. 1993. Geometry of flow paths for fluid transport in rocks. *Journal of Geophysical Research* 98(B7): 12267–12278.

Durham WB, Bonner BP. 1994. Self-propping and fluid flow in slightly offset joints at high effective pressures. *Journal of Geophysical Research* 99(B5): 9391–9399.

Fourar M, Lenormand R. 2001. A new model for two-phase flows at high velocities through porous media and fractures. *Journal of Petroleum Science and Engineering* 30: 121–127.

Ge S. 1997. A governing equation for fluid flow in rough fractures. *Water Resources Research* 33(1): 53–61.

Hasegawa E, Izuchi H. 1983. On the steady flow through a channel consisting of an uneven wall and a plane wall. *Bulletin of the Japan Society of Mechanical Engineers* 26: 514–520.

Iwai K. 1976. Fundamental studies of the fluid flow through a single fracture. PhD thesis, University of California, Berkeley, California.

Keller AA, Roberts PV, Kitanidis PK. 1995. Prediction of single phase transport parameters in a variable aperture fracture. *Geophysical Research Letter* 22(11): 1425–1428.

Konzuk JS, Kueper BH. 2004. Evaluation of cubic law based models describing single-phase flow through a rough-walled fracture. *Water Resources Research* 40: W02402. DOI: 10.1029/2003WR002356.

Koyama T, Neretnieks I, Jing L. 2008. A numerical study on differences in using Navier–Stokes and Reynolds equations for modeling the fluid flow and particle transport in single rock fractures with shear. *International Journal of Rock Mechanics and Mining Sciences* 45: 1082–1101.

Lomize GM. 1951. *Flow in Fractured Rocks (in Russian)*, Gosenergoizdat: Moscow, USSR.

Louis C. 1969. A study of groundwater flow in jointed rock and its influence on the stability of rock masses. *Imperial College Rock Mechanics Research Report* 10: 90.

Meheust Y, Schmittbuhl J. 2001. Geometrical heterogeneities and permeability anisotropy of rough fractures. *Journal of Geophysical Research* 106(B2): 2089–2102.

Moreno L, Tsang YW, Tsang CF, Hale FV, Neretnieks I. 1988. Flow and tracer transport in a single fracture: a stochastic model and its relation to some field observations. *Water Resources Research* 24: 2033–2048.

Mourzenko VV, Thovert JF, Adler PM. 1995. Permeability of a single fracture: validity of the Reynolds equation. *Journal of Physics II France* 5: 465–482.

Munson BR, Young DF, Okiishi TH. 1998. *Fundamentals of Fluid Mechanics*, 3rd edn, Wiley: New York.

Nazridoust K, Ahmadi G, Smith DH. 2006. A new friction factor correlation for laminar, single-phase flows through rock fractures. *Journal of Hydrology* 329: 315–328.

Nowamooz A, Radilla G, Fourar M. 2009. Non-Darcian two-phase flow in a transparent replica of a rough-walled rock fracture. *Water Resources Research* 45: W07406. DOI: 10.1029/2008WR007315.

Oron AP, Berkowitz B. 1998. Flow in fractures: the local cubic law assumption reexamined. *Water Resources Research* 34(11): 2811–2825.

Pyrak-Nolte LJ, Myer LR, Cook NGW, Witherspoon PA. 1987. Hydraulic and mechanical properties of natural fractures in low permeability rock. In *Proceedings of 6th International Congress on Rock Mechanics*. Montreal, Canada, 30 August 1987; 225–231.

Qian J, Liu Y, Wang J, Guan H, Chen S, Wang J. 2006. Non-LCL and tracer test for groundwater flow in a single fracture. *Journal of Hydrodynamics Series B* 18(1): 104–108.

Qian J, Zhan H, Luo S, Zhao W. 2007. Experimental evidence of scale-dependent hydraulic conductivity for fully developed turbulent flow in a single fracture. *Journal of Hydrology* 339: 206–215.

Qian J, Zhan H, Zhao W, Sun F. 2005. Experimental study of turbulent unconfined groundwater flow in a single fracture. *Journal of Hydrology* 311: 134–142.

Ranjith PG, Darlington W. 2007. Nonlinear single-phase flow in real rock joints. *Water Resources Research* 43: W09502. DOI: 10.1029/2006WR005457.

Raven KG, Gale JE. 1985. Water flow in a natural rock fracture as a function of stress and sample size. *International Journal of Rock Mechanics and Mining Sciences and Geomechanics Abstracts* 22(4): 251–261.

Schrauf TW, Evans DD. 1986. Laboratory studies of gas flow through a single natural fracture. *Water Resources Research* 22: 1038–1050.

Sisavath S, Al-Yaarubi A, Pain CC, Zimmerman RW. 2003. A simple model for deviations from the cubic law for a fracture undergoing dilation or closure. *Pure and Applied Geophysics* 160: 1009–1022.

Skjetne E, Hansen A, Gudmundsson JS. 1999. High-velocity flow in a rough fracture. *Journal of Fluid Mechanics* 383: 1–28.

Thompson ME, Brown SR. 1991. The effect of anisotropic surface roughness on flow and transport in fractures. *Journal of Geophysical Research* 96(B13): 21923–21932.

Tsang YW. 1992. Usage of "Equivalent apertures" for rock fractures as derived from hydraulic and tracer tests. *Water Resources Research* 28(5): 1451–1455.

Unger AJA, Mase CW. 1993. Numerical study of the hydromechanical behavior of two rough fracture surfaces in contact. *Water Resources Research* 29: 2101–2114.

Vandergraaf TT. 1995. Radionuclide migration experiments under laboratory conditions. *Geophysical Research Letter* 22(11): 1409–1412.

Wen Z, Huang G, Zhan H. 2006. Non-Darcian flow in a single confined vertical fracture toward a well. *Journal of Hydrology* 330: 698–708.

Witherspoon PA, Wang JSY, Iwai K, Gale JE. 1980. Validity of cubic law for fluid flow in a deformable rock fracture. *Water Resources Research* 16(6): 1016–1024.

Xu G, Zhang Y, Ha Q. 2003. Super-cubic and sub-cubic law of rough fracture seepage and its experiments study (in Chinese). *Journal of Water Conservancy* 3: 74–79.

Zimmerman RW, Al-Yaarubi AH, Pain CC, Grattoni CA. 2004. Nonlinear regimes of fluid flow in rock fractures. *International Journal of Rock Mechanics and Mining Sciences* 41: 1A27.

Zimmerman RW, Bodvarsson GS. 1996. Hydraulic conductivity of rock fractures. *Transport in Porous Media* 23: 1–30.

Zimmerman RW, Kumar S, Bodvarsson GS. 1991. Lubrication theory analysis of the permeability of rough-walled fractures. *International Journal of Rock Mechanics and Mining Sciences and Geomechanics Abstracts* 28(4): 325–331.

Zimmerman RW, Yeo IW. 2000. Fluid flow in rock fractures: from the Navier–Stokes equations to the cubic law. In *Dynamics of Fluids in Fractured Rock*, Faybishenko B, Witherspoon PA, Benson SM (eds). American Geophysical Union Monograph 122: Washington, DC; 213–224.